Transport properties of lithium hydride from quantum molecular dynamics and orbital-free molecular dynamics

D. A. Horner,[1] F. Lambert,[2] J. D. Kress,[1] and L. A. Collins[1]
[1]*Theoretical Division, Los Alamos National Laboratory, Los Alamos, New Mexico 87545, USA*
[2]*CEA, DAM, DIF, F-91297 Arpajon, France*
(Received 30 April 2009; revised manuscript received 24 June 2009; published 16 July 2009)

We have performed a systematic study of lithium hydride in the warm-dense-matter regime for a density range from one to four times ambient solid and for temperatures from 2 to 6 eV using both finite-temperature density-functional theory quantum molecular dynamics (QMD) and orbital-free molecular dynamics (OFMD) with a focus on dynamical properties such as diffusion and viscosity. The validity of various mixing rules, especially those utilizing pressure, were checked for composite properties determined from QMD/OFMD simulations of the pure species against calculations on the fully interacting mixture. These rules produce pressures within about 10% of the full-mixture values but mutual-diffusion coefficients as different as 50%. We found very good agreement overall between the QMD, employing a three-electron pseudopotential, and the OFMD in the local-density approximation, especially at the higher temperatures and densities.

DOI: 10.1103/PhysRevB.80.024305 PACS number(s): 66.20.Cy, 52.25.Fi

I. INTRODUCTION

Mixtures span a wide variety of material states from diffuse gases at room temperature to highly compressed fluids at millions of degrees and play a particularly important role in the regime of warm dense matter (WDM). This regime ranges in temperatures from a few thousand ($\sim$1 eV) to a few million ($\sim$100 eV) degrees Kelvin and in densities from a few hundredths solid ($\sim 10^{21}$ atoms/cm^3) to hundreds of times compressed solid ($\sim 10^{25}$ atoms/cm^3). WDM in turn encompasses a diverse set of environments and phenomena such as the interiors of exoplanets around distant starts,[1,2] the atmospheres of White Dwarfs,[3] the compression phase of an inertial confinement fusion (ICF) capsule,[4] and the plasma produced in the interaction of an ultrafast, high-intensity laser pulse with a solid.[5,6] In the exoplanets, the equation of state of a mixture of Hydrogen and Helium determines the distribution in size and structure[7,8] while for White Dwarfs, the same constituents govern the opacity, which forms an important component in setting the cooling rates and in turn the efficacy of these objects as astrochronometers. For the ICF capsules, the mixing of impurities such as plastics, Beryllium, or Copper from the various layers into the Deuterium/Tritium fuel can have a considerable impact on the burn efficiency. The laser bombardment of materials as varied as atomic clusters, nanostructures, and solids together with intricate diagnostic tools can yield important insights into the nature of the chemical binding, the melting process, and the transport of energy. The accuracy of the macroscopic modeling of these environments rests strongly on a detailed knowledge of the underlying microscopic properties such as equation of state (EOS), diffusion, and opacities.

In a previous paper,[9] we selected lithium hydride (LiH) as a representative system and examined some of the standard mixing rules with respect to the EOS and optical properties in the WDM regime. The properties of the full mixture and the individual pure species derived from quantum molecular-dynamics (QMD) simulations, which treated the electrons quantum mechanically through finite-temperature density-functional theory (FTDFT) and the nuclei classically. The results agreed with the trends found in studies[10–12] of other mixtures in this regime, mainly, that for the EOS, rules based on matching the pressures yielded reasonable agreement with full-mixture simulations. However, although the integrated opacities showed similar agreement, the frequency-dependent absorption coefficients displayed large differences in certain frequency ranges between the composite from the mixing rules and the complete mixture. These differences could have important consequences for large-scale radiation-hydrodynamical simulations. In this paper, we extend these studies to dynamical properties such as diffusion and viscosity and in addition to the FTDFT, employ an orbital-free molecular-dynamics (OFMD) approach. In the next section, we present an overview of the formalism and parameters employed in the simulations, followed in Sec. III by a presentation and comparison of results from the various approaches. Finally, the last section contains a summary of the findings.

II. FORMALISM

In this section, we present only a brief description of the basic formalism employed to explore mixtures in the WDM regime since more comprehensive expositions appear elsewhere as indicated in the citations. Two basic quantum-mechanical density-functional approaches, one based on Kohn-Sham (KS) and the other on orbital free, form the basis of our simulations. We also discuss the implementation of various schemes to determine the dynamical properties such as diffusion and viscosity. The final part treats the mixing rules that combine pure-species quantities to form composite properties.

A. Quantum molecular dynamics

We have performed QMD simulations for LiH using the Vienna *ab initio* Simulation Package (VASP).[13–15] In these simulations, the electrons are treated fully quantum mechani-

 ©2009 The American Physical Society

cally by employing a plane-wave FTDFT description. The electron-ion interaction is represented by a projector-augmented wave (PAW) pseudopoential. The ions are evolved classically according the forces from the electron-density and the ion-ion repulsion. The system was assumed to be in local thermodynamic equilibrium with the electron and ion temperatures being equal ($T_e=T_i$). In our simulations, the electron temperature was fixed in the FTDFT and the ion temperature was kept constant through simple velocity rescaling.

At each time step t for a periodically replicated cell of volume (V) containing N_e active electrons and N_i ions in fixed spatial positions $\mathbf{R}_q(t)$, we first perform a FTDFT calculation within the KS construction[16] to determine a set of electronic state functions $[\Psi_{i,\mathbf{k}}(\mathbf{r},t)|i=1,n_b]$ for each k-point $\mathbf{k}$

$$H_{\mathrm{KS}}\Psi_{i,\mathbf{k}}(\mathbf{r},t)=\epsilon_{i,\mathbf{k}}\Psi_{i,\mathbf{k}}(\mathbf{r},t) \tag{1}$$

with $\epsilon_{i,\mathbf{k}}$, the eigenenergy and

$$H_{\mathrm{KS}}=-\frac{1}{2}\nabla^2+V_{\mathrm{ext}}(\mathbf{r})+\int\frac{n(\mathbf{r}')}{|\mathbf{r}-\mathbf{r}'|}\mathrm{d}\mathbf{r}'+v_{\mathrm{xc}}(\mathbf{r}) \tag{2}$$

(in atomic units) with

$$n(\mathbf{r})=2\sum_i|\Psi_{i,\mathbf{k}}(\mathbf{r},t)|^2. \tag{3}$$

The terms represent, respectively, the kinetic energy; the external or electron-ion interaction, which can include pseudopotentials; the Hartree contribution; and the exchange-correlation potential.

The ions are then advanced with a velocity Verlet algorithm, based on the force from the ions and electronic density, to obtain a new set of positions and velocities. Repeating these two steps propagates the system in time yielding a trajectory consisting of the positions and velocities $[\mathbf{R}_q(t),\mathbf{V}_q(t)]$ of the ions and a collection of state functions $[\Psi_{i,\mathbf{k}}(\mathbf{r},t)]$ for the electrons.

All simulations employed only Γ-point ($\mathbf{k}=0$) sampling of the Brillouin Zone and 216 atoms; 108 atoms each of H and Li in a cubic cell of length L (volume $V=L^3$). We solve the KS equations within the generalized gradient approximation and described the hydrogen-electron interaction by a PAW with a maximum energy cutoff (E_{max}) of 400 eV while, for lithium, we employed both a single-electron (PAW-1e) and a full-electron (PAW-3e) PAW also with $E_{\mathrm{max}}=400$ eV. A sufficient number of bands n_b were included so that the occupation of the highest band was less than 10^{-3}. Trajectories were generally evolved for 0.25 ps with time steps of 0.5 fs when $T=2$ eV and time steps of 0.25 fs when $T>2$ eV although longer examples were employed as a check.

B. Orbital-free molecular dynamics

We also investigated LiH under the same conditions using OFMD simulations.[17–19] In this scheme, the kinetic energy of the electrons is treated in a semiclassical approximation. The semiclassical expansion up to first order of the partition function of the electrons leads to the well-known Thomas-Fermi expression,[20] the first term in Eq. (4), which depends only on the local electronic density in the true spirit of the Hohenberg-Kohn theorem.[21] The second term in the expansion gives the Von Weiszäcker correction to the free energy. Therefore, the orbital-free electronic free energy reads as

$$\begin{aligned}F^e[\mathbf{R},n]=&\frac{1}{\beta}\int\mathrm{d}\mathbf{r}\left\{n(\mathbf{r})\Phi[n]-\frac{2\sqrt{2}}{3\pi^2\beta^{3/2}}I_{3/2}[\Phi(n)]\right\}+F^{\mathrm{xc}}[n]\\&+\frac{1}{2}\int\int\mathrm{d}\mathbf{r}\mathrm{d}\mathbf{r}'\frac{n(\mathbf{r})n(\mathbf{r}')}{|\mathbf{r}-\mathbf{r}'|}+\sum_{\ell=1}^{N_a}Z_\ell\int\mathrm{d}\mathbf{r}\frac{n(\mathbf{r})}{|\mathbf{r}-\mathbf{R}_\ell|}\\&-\mu\int\mathrm{d}\mathbf{r}\left[n(\mathbf{r})-\sum_{\ell=1}^{N_a}Z_\ell\right],\end{aligned} \tag{4}$$

where I_ν is the Fermi integral of order ν and Φ is an implicit functional of n determined by charge conservation through

$$\sum_{\ell=1}^{N_a}Z_\ell=\frac{\sqrt{2}}{\pi^2\beta^{3/2}}\int\mathrm{d}\mathbf{r}I_{1/2}(\Phi[n]). \tag{5}$$

The exchange-correlation term $F^{\mathrm{xc}}[n]$ in Eq. (4) is expressed in the local-density approximation of Perdew and Zunger.[22] For this study, we omit the Von Weiszäcker correction and work in a Thomas-Fermi-Dirac (TFD) form using the formula proposed by Perrot[23] to deal with kinetic-entropic part. The divergence of the electron-nucleus potential is regularized at each thermodynamic condition through a procedure that closely follows the production of norm-conserving pseudopotential for QMD.[24] The cutoff radius is chosen to be 30% of the Wigner-Seitz radius preventing the overlap of regularization spheres. The number of plane waves to describe the local electronic density is then adjusted to get convergence of the thermodynamic properties within less than one percent.

The chain of calculation of the OFMD procedure is similar to the QMD one. At each time step, the electronic free energy is minimized in terms of the local electronic density and nuclei are propagated according to their electrostatic interactions arising from both nuclei and electrons. The molecular dynamics is performed in the isokinetic ensemble and the time step is computed from the thermal velocity of the nuclei and the Wigner-Seitz radius.[25] We insist here that the classical particles are nuclei and not ions as in standard QMD (except all electron simulations). The orbital-free procedure deals—approximately—with all electrons on an equal footing, there are no notions such as core, valence, or ionized electrons. All the electrons are collectively represented by the local electronic density $n(\mathbf{r})$.

For the purposes of this paper, we shall use the symbol "QMDα" to represent simulations with the finite-temperature density-functional-theory molecular-dynamics formulation in the Kohn-Sham orbital mode with PAW potentials with the one-electron ($\alpha=1$) or the three-electron ($\alpha=3$) forms for Li. By "OFMD," we shall refer to the orbital-free molecular-dynamics formulation with regularized electron-ion potentials in the Thomas-Fermi-Dirac mode.

C. Static and transport properties

In this section, we present only a brief summary of the basic static and dynamical properties determined in our simulations since detailed expositions appear elsewhere.[26–28]

The total pressure of the system

$$P = \frac{Nk_BT}{V} + P_e \tag{6}$$

is the sum of the ideal-gas pressure of the ions and the excess pressure P_e, computed via the electronic forces from the DFT calculation. The excess pressure is averaged over the trajectory after the system has been equilibrated.

The self-diffusion coefficient D_α for species α is computed from the trajectory for the mean-square displacement

$$D_\alpha = \frac{1}{6t}\langle|\mathbf{R}_i(t) - \mathbf{R}_i(0)|^2\rangle \tag{7}$$

or by the velocity autocorrelation function

$$D_\alpha = \frac{1}{3}\int_0^\infty \langle \mathbf{V}_i(t)\cdot\mathbf{V}_i(0)\rangle \mathrm{d}t, \tag{8}$$

where $\mathbf{R}_i$ ($\mathbf{V}_i$) is the position (velocity) of the ith particle of species α. This quantity is computed for both Li and H.

These two formations for the self-diffusion coefficients are only formally equivalent in the long-time limit. We have generated MD trajectories of sufficient temporal length to reach this regime in which the velocity autocorrelation function becomes zero and contributes no further to the integral and the mean-square displacement away for the origin consistently fits to a straight line. The values obtained from these two approaches generally lie with one percent of each other; we therefore report only one value.

Also, we have computed the mutual-diffusion coefficient $D_{\alpha\beta}$ from the autocorrelation function

$$D_{\alpha\beta} = \frac{Q}{3Nx_\alpha x_\beta}\int_0^\infty \langle A(0)A(t)\rangle \mathrm{d}t \tag{9}$$

with

$$A(t) = x_\beta \sum_{i=1}^{N_\alpha} \mathbf{v}_i(t) - x_\alpha \sum_{j=1}^{N_\beta} \mathbf{v}_j(t). \tag{10}$$

The thermodynamic factor Q was taken to be unity and x_α and N_α represent the concentration and particle number of species α, respectively, $(N=\Sigma_\alpha N_\alpha)$.

The viscosity was computed from the autocorrelation function of the off-diagonal component of the stress tensor[26]

$$\eta = \lim_{t\to\infty} \bar{\eta}(t), \tag{11}$$

where

$$\bar{\eta}(t) = \frac{V}{k_BT}\int_0^t \langle P_{12}(0)P_{12}(t')\rangle \mathrm{d}t'. \tag{12}$$

We averaged the results for the five independent off-diagonal components of the stress tensor P_{xy}, P_{yz}, P_{zx}, $(P_{xx}-P_{yy})/2$, and $(P_{yy}-P_{zz})/2$.

Finally, the radial distribution function (RDF) $g_{\alpha\beta}(r)$ between two constituents, given by

$$g_{\alpha\beta}(r) = \frac{V}{N^2}\left\langle \sum_i \sum_j \delta[r - r_{ij}] \right\rangle, \tag{13}$$

describes the basic structure of the fluid. The term r_{ij} represents the radial separation between the ith atom of species α and the jth atom of species β.

D. Mixing rules

As in the case with the static and optical properties,[9] we examine two representative mixing rules. The first, termed density-matching (MRd), draws its inspiration from a two-species ideal gas while the second, termed pressure-matching mixing rules (MRp), follows more from two interacting immiscible fluids.

In the MRd, we have set the volume of the individual species to that of the total mixture $[V_H = V_{Li} = V_{LiH}]$ and performed QMD/OFMD simulations for H at a density of N_H/V_{LiH} and Li at N_{Li}/V_{LiH} at a fixed temperature T. We then determine a total pressure by simply adding the individual pressures from the separate H and Li simulations. Other composite properties such as mutual diffusion and viscosity follow the same prescription. The MRd can be summarized as

$$\begin{aligned} V_{LiH} &= V_H = V_{Li}, \\ P^d_{LiH} &= P_H + P_{Li} \\ D^d_{LiH} &= D_H + D_{Li} \\ \eta^d_{LiH} &= \eta_H + \eta_{Li}. \end{aligned} \tag{14}$$

We have added a superscript to designate properties derived from a particular mixing rule as opposed to those for the full mixture. For the pressure, the density mixing rule basically follows an ideal-gas prescription for noninteracting Li and H gases in a volume V_{LiH}.

The MRp involves a more complicated construction. In this case, we must perform a series of QMD/OFMD simulations on the individual species in which the volumes are varied under the constraint $[V^p_{LiH} = V_H + V_{Li}]$ until the individual pressures agree $[P_H = P_{Li}]$. The total pressure becomes P_H (or equally P_{Li}). Composite properties such as mutual diffusion and viscosity are determined by combining the individual species results according to the volume fractions $[v_\alpha = V_\alpha/V_{LiH}]$. The MRp then consists of the following prescription:

$$\begin{aligned} V_{LiH} &= V_H + V_{Li} \\ P^p_{LiH} &= P_H[V_H, T] = P_{Li}[V_{Li}, T] \\ D^p_{LiH} &= v_H D_H + v_{Li} D_{Li} \\ \eta^p_{LiH} &= v_H \eta_H + v_{Li}\eta_{Li}. \end{aligned} \tag{15}$$

We use throughout the excess or electronic pressure P_e to evaluate this mixing rule.

Finally, we also draw from binary ionic mixture (BIM) studies and derive composite properties from a slightly more complex rule[10]

$$\sum_i v_i \frac{\gamma_i - \gamma_m}{\gamma_i + \frac{3}{2}\gamma_m} = 0 \tag{16}$$

with γ representing either the mutual-diffusion coefficient or the viscosity. The subscript m denotes the full mixture and i, the pure species.

We should emphasize that the comparison of the above mixing rules represents a "best case scenario" since the properties of the individual species themselves originate from QMD calculations. While divorced of the LiH interactions, these pure-species simulations still encompass complex intra-atomic interactions over large samples of atoms. In many mixture studies, the properties of pure species derive from perturbed-atom models, which treat a single representative atom within a cell whose boundary conditions are adjusted to introduce effects from the surrounding medium. These "average atom" models[29] approximate to some extent the environments of the fluid state experienced by the pure species in the QMD simulations.

III. RESULTS AND DISCUSSION

We present the wealth of information derived from our calculations mainly through tables and figures and concentrate in the text on general trends and representative cases. We explore LiH mixtures in a regime of more extreme conditions than our previous study[9] and examine densities from one (0.7874 g/cm^3) to four times solid and temperatures from 2 (~20 kK) to 6 eV (~70 kK). Before analyzing the results of the QMD and OFMD calculations, we focus on several procedural points that underlie the computation of the various static and dynamical properties.

A. Preliminaries

1. Choice of PAW for QMD simulations

Since the density reaches a factor of four larger than that of solid LiH, the validity of the PAW construction, generally performed at natural material conditions, requires careful examination, especially for Li. The PAW forms available come in two flavors: (1) PAW-1e that utilizes only the valence 2*s* electron and (2) PAW-3e that models all three electrons. Since the computational time for the QMD scales as the number of active electrons, the one-electron formulation has distinct advantages for the long-time propagations required to converge the viscosity and mutual-diffusion coefficients. However, our findings indicate that for compressions above solid, the application of PAW-1e merits some caution. As an example, Fig. 1 compares the self-diffusion coefficients for Li as a function of density and temperature for the one-electron (solid line) and three-electron (dotted line) PAW potentials. Only at the lowest temperature and density do the results show reasonable agreement, varying by about 10%. For more compressed and hotter conditions, the differences rapidly increase, reaching the 100% level above three times

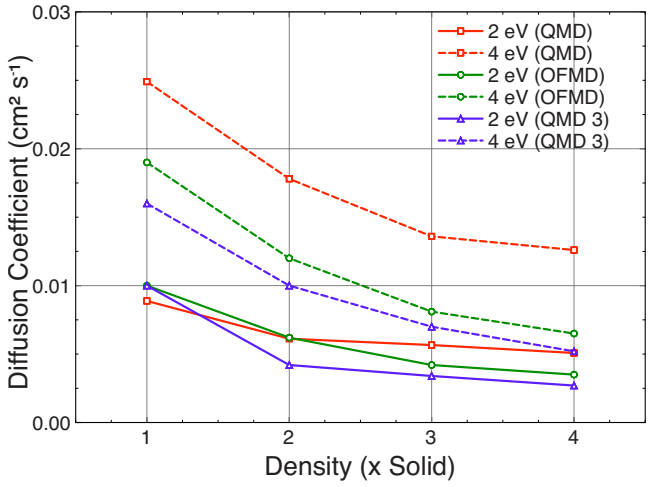

FIG. 1. (Color online) Self-diffusion coefficient for Li as a function of density for isotherms at 2 eV (solid line) and 4 eV (dashed line) and for different potential forms: (1) VASP PAW-1e (square/red), (2) VASP PAW-3e (triangle/blue), and (3) OFMD (circle/green).

solid density. The electronic pressure and self-diffusion of H fare better with disagreements generally in a 10–20 % range over the entire ρ-T space covered. The latter may arise from our choice of a hard H PAW. We have included the OFMD results as a reference.

We probe the origins of these differences further by examining the radial distribution functions $g(r)$ between the various constituents, especially the Li atoms, for the full LiH mixture. The upper panel of Fig. 2 for solid density shows a general agreement between the RDFs from the one- and three-electron PAWs at 2 eV except at very small separations ($<$1.2 Å), which accounts for the small differences in the pressure and diffusion coefficients. However, even at this density for the higher temperature (4 eV), a significant disparity arises in D_{Li}. As the density increases (lower panel), this disparity becomes further magnified as witnessed by the large span in the RDFs between the PAW forms. The one-electron PAW allows significantly closer approaches of the Li atoms than the full three-electron potential with significant ramifications for the dynamical properties. This could arise from a poor representation of the very compacted 1*s* Li core, implying that the one-electron PAW is too "soft" or from significant overlap and interplay of the Li 1*s* orbitals. Electronic-structure calculations[30] of the lithium dimer [Li_2] find that the 1*s* cores only significantly overlap once the internuclear separation becomes smaller than about 1 Å. Even for the densest case, the atoms remain generally separated beyond this core region as indicated by the three-electron PAW results. A comparison with the OFMD results further supports these conclusions. The OFMD potential is constructed anew for each density and temperature and reflects changes in the short-range region. These findings corroborate the conclusions reached by Mazevet *et al.*[18] on the design of pseudopotentials for highly compressed boron. On the other hand, the RDF for H-H shows little sensitivity to the choice of Li PAW, a fact reflected in the smaller differences in the hydrogen self-diffusion. Therefore, we generally

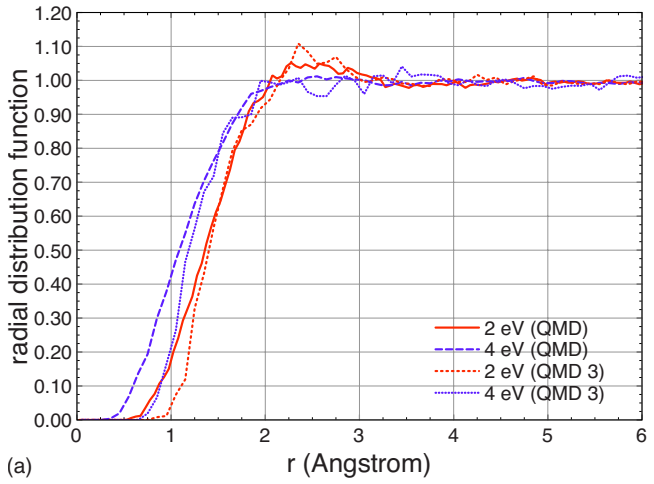

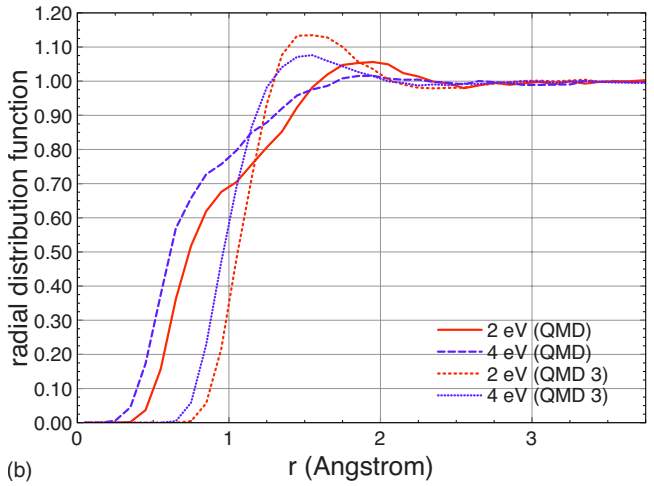

FIG. 2. (Color online) Radial distribution functions for Li-Li as a function of separation distance r at solid (upper panel) and four times solid (lower panel) density and temperatures of 2 (solid) and 4 eV(dot). Comparison of potential forms: (1) PAW-1e (QMD1) and (2) PAW-3e (QMD3).

employ the three-electron form; however, a "harder" one-electron psesudopotential would likely also give reasonable results with less computational costs.

2. Calculation of the mutual-diffusion and viscosity coefficient

Unlike the self-diffusion coefficient, which involves single-particle correlations and attains significant statistical improvement from averaging over the particles, the viscosity, and mutual diffusion depend on the entire system and therefore require very long trajectories in order to gain statistical accuracy. We have found that the use of empirical fits to the integrals of the autocorrelation functions can substantially shorten the length of the trajectory required. In turn, extrapolation of the fits to much longer times can more effectively determine the basic dynamical property. In Fig. 3 we give an example of the fitting procedure for the viscosity at three times solid density and a temperature of 4 eV. The partial integral of the off-diagonal stress-tensor autocorrelation function, $\bar{\eta}(t)$, has been fit to the functional form $A[1-\exp(-t/\tau)]$, where A and τ are free parameters

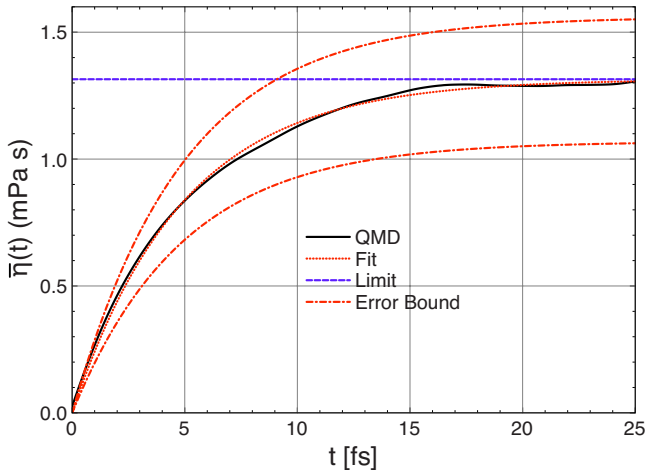

FIG. 3. (Color online) Fit of partial integral of the off-diagonal stress-tensor autocorrelation function, $\bar{\eta}(t)$ for 3× solid and 4 eV.

with A giving the reported quantity. Fitting to this form at short-time integrations may produce a reasonable approximation to the η; the procedure also aids in damping the long-time variation. The statistical error inherent in computing correlation functions from molecular-dynamics trajectories[31] is $\sqrt{2\tau/T}$, where T is the length of the trajectory and τ is the correlation or e-folding time of the function, calculated either directly from the fit or from an interrogation of the function itself. We generally fit over a time interval of $[0,4\tau-5\tau]$. In Fig. 3, the curves labeled "Error Bound" display the range of error around the fit due to the autocorrelation statistics. This particular example employed a trajectory of length of 10 000 and a correlation time of 200 time steps of length 0.25 fs. Typically, trajectories of this length sufficed for 4 and 6 eV while less steps (~5000) of longer

TABLE I. Comparison of excess (electronic) pressure between quantum molecular dynamics for a single-electron (QMD1) and three-electron (QMD3) PAW for Li and the OFMD in the TFD mode as a function of density relative to the solid LiH and temperature.

ρ (× Solid)	T (eV)	P_e (GPa)		
		QMD1	QMD3	OFMD
1	2	31	32	38
	4	57	59	66
	6			100
2	2	127	141	147
	4	174	196	204
	6	229	258	271
3	2	286	335	333
	4	350	420	419
	6	428	512	519
4	2	497	626	609
	4	575	740	721
	6	671	860	851

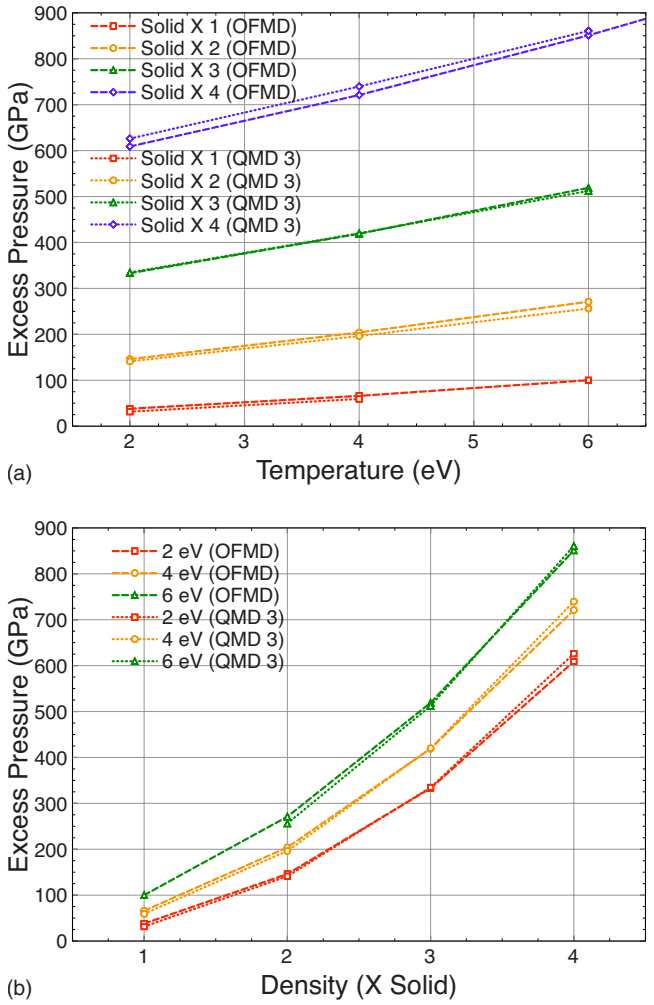

FIG. 4. (Color online) Excess pressure P_e as a function of temperature and density (top and bottom panels, respectively).

duration (0.5 fs) accommodated lower temperature. The trajectory length showed greater sensitivity to temperature than density as expected. For the viscosity and mutual-diffusion coefficients, the error computed in this way, $\sqrt{2\tau/T}$, is 30% or less, except for the viscosity at $1\times$Solid and 4 eV where the error is 50%. On the other hand, the error for the self-diffusion remains at less than 5% since the particle average introduces an additional $1/\sqrt{N}$ advantage.

B. Comparison of QMD and OFMD simulations

1. Pressure

In Table I and Fig. 4, we present the electronic (excess) pressure P_e of the LiH mixture as a function of compression and temperature for the QMD with PAW-1e and PAW-3e and for the OFMD. The difference between the two PAW potentials is fairly small with the largest disparity $[|P_e(\text{PAW-1e})-P_e(\text{PAW-3e})|/P_e(\text{PAW-3e})\sim 20\%]$ occurring at the highest density and temperature. For the solid density, the QMD3 (PAW-3e) and the OFMD show their greatest disagreement but only about 20% for lowest temperature. As the density rises, the agreement becomes extremely close ($<5\%$) and within the statistical errors for these simulations. At the lowest density, transient molecular effects linger, requiring the full DFT representation. However, with increasing density, the electrons have a more uniform distribution throughout the sample and the orbital free becomes a reasonable representation.

2. Self-diffusion

In Table II and Figs. 5 and 6, we present a comparison of the QMD and OFMD simulations for the self-diffusion coefficient for hydrogen (D_{H}) and lithium (D_{Li}) as a function of density and temperature from two perspectives. Once again, we observe good agreement between the QMD3 (PAW-3e) and the OFMD results.

TABLE II. Comparison of self and mutual-diffusion coefficients for QMD and OFMD as a function of density and temperature. Method labels same a Table I. Numbers in square brackets represent powers of ten.

		D_{H} ($\mathrm{cm/s^2}$)			D_{Li} ($\mathrm{cm/s^2}$)			D_{LiH} ($\mathrm{cm/s^2}$)	
ρ ($\times$ Solid)	T (eV)	QMD1	QMD3	OFMD	QMD	QMD3	OFMD	QMD	OFMD
1	2	3.4[−2]	2.9[−2]	2.7[−2]	8.9[−3]	8.5[−3]	1.0[−2]	2.2[−2]	3.4[−2]
	4	7.1[−2]	6.5[−2]	6.1[−2]	2.5[−2]	1.6[−2]	1.9[−2]	3.2[−2]	3.6[−2]
	6			1.1[−1]			3.2[−2]		5.2[−2]
2	2	1.5[−2]	1.4[−2]	1.4[−2]	6.1[−3]	4.2[−3]	6.2[−3]	9.5[−3]	9.2[−3]
	4	3.4[−2]	3.0[−2]	3.3[−2]	1.8[−2]	1.0[−2]	1.2[−2]	2.2[−2]	3.3[−2]
	6	6.0[−2]	5.4[−2]	5.6[−2]	2.8[−2]	1.5[−2]	1.6[−2]	3.6[−2]	4.5[−2]
3	2	1.0[−2]	9.4[−3]	9.3[−3]	5.7[−3]	3.4[−3]	4.2[−3]	6.1[−3]	8.5[−3]
	4	2.3[−2]	2.3[−2]	2.1[−2]	1.4[−2]	7.2[−3]	8.1[−3]	1.6[−2]	1.9[−2]
	6	4.2[−2]	3.6[−2]	3.9[−2]	2.1[−2]	1.1[−2]	1.2[−2]	2.8[−2]	3.0[−2]
4	2	7.8[−3]	6.8[−3]	7.7[−3]	5.1[−3]	2.7[−3]	3.5[−3]	4.6[−3]	4.2[−3]
	4	1.8[−2]	1.6[−2]	1.8[−2]	1.3[−2]	5.2[−3]	6.4[−3]	1.2[−2]	1.1[−2]
	6	3.2[−2]	2.3[−2]	2.8[−2]	2.0[−2]	8.9[−3]	1.0[−2]	2.5[−2]	2.2[−2]

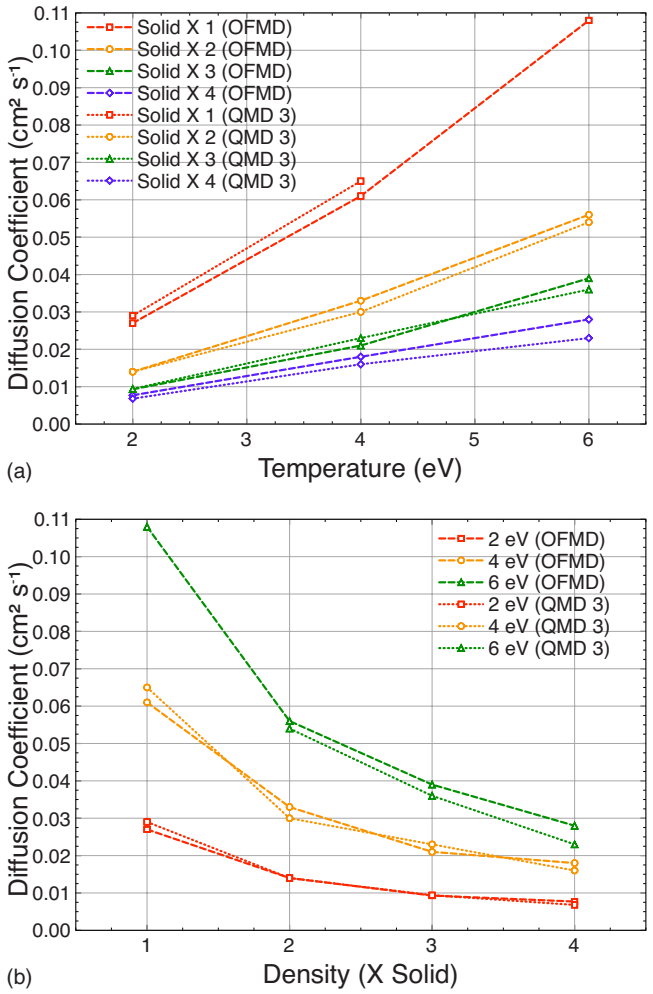

FIG. 5. (Color online) Self-diffusion coefficient for hydrogen as a function of temperature and density (top and bottom panels, respectively).

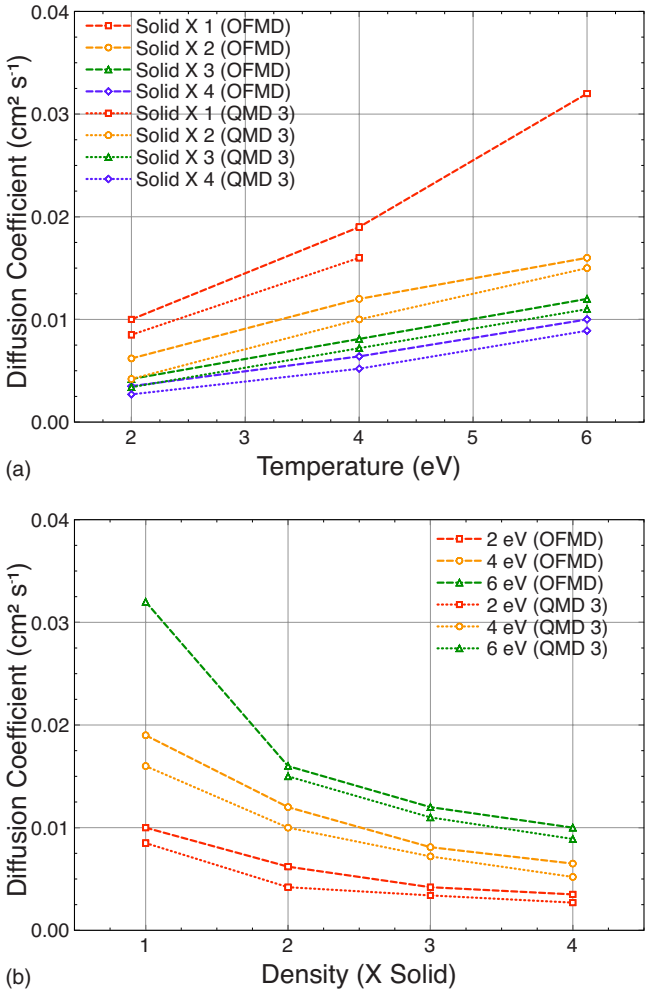

FIG. 6. (Color online) Self-diffusion coefficient for lithium as a function of temperature and density (top and bottom panels, respectively).

For a fixed density, the self-diffusion coefficient rises with temperature as the atoms become more mobile. On the other hand, for a given temperature, the diffusion declines with increasing density, reflecting the greater confinement of the atoms. The lithium self-diffusion displays the largest differences between the two approaches with the low-temperature regime generally showing the greatest disparities. At the higher temperatures, the disagreements stay within the 10% realm. For hydrogen, the situation is even better, with results less than 10% across except at the very highest density and temperature (23%). We observe an important trend that in general D_{H} remains a factor of two to three larger than D_{Li} over the entire range of temperature and density. This indicates that for the LiH mixture that hydrogen plays a dominant role in the dynamics.

3. Mutual diffusion and viscosity

Due to the long trajectories required in determining the mutual diffusion and viscosity, we have only made calculations in the QMD for the one-electron pseudopotential (PAW-1e). This together with poorer statistics inherent in the determination of these properties implies a less quantitative comparison. However, within these limitations, we can still gain an understanding of the basic behavior of these dynamical quantities and the validity of the various formulations. The last two columns of Table II and Fig. 7 display the mutual-diffusion coefficient for the QMD1 and OFMD as a function of temperature and density. We find the QMD and OFMD generally in agreement (20% or better) for the higher densities and temperatures. The upper panel of Fig. 7 presents the trend in D_{LiH} for a fixed density as the temperature varies. For the higher densities [3× and 4× Solid], the two methods give similar behavior and remain in good agreement. A break occurs around twice solid density with the curves remaining parallel but much further apart.

For the mutual-diffusion coefficient, a particularly simple combination rule exists based on dilute mixtures for which the cross-correlation terms are negligible[27]

$$D_{\mathrm{LiH}} = Q[x_{\mathrm{H}} D_{\mathrm{H}} + x_{\mathrm{Li}} D_{\mathrm{Li}}] \tag{17}$$

with x_i the mole fraction for species i. The thermodynamical factor Q is set to unity. This formula is not a mixing rule per se but an approximation of Eq. (9) in which cross terms are neglected. The self-diffusion coefficients come from the evo-

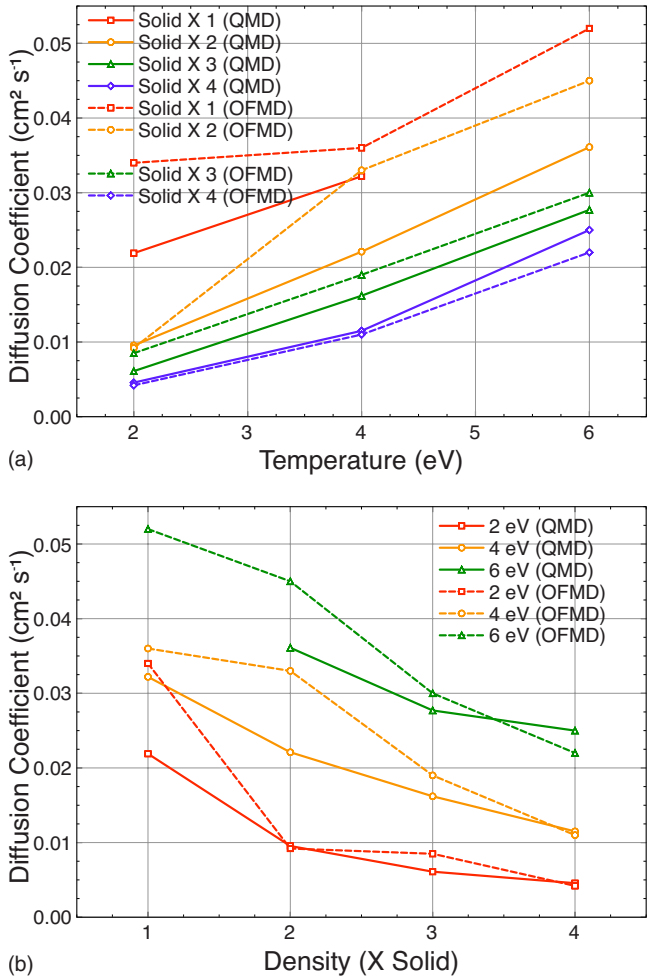

FIG. 7. (Color online) Mutual-diffusion coefficient as a function of temperature and density (top and bottom panels, respectively).

lution of the *full* LiH mixture, not from results on individual pure species. Since self-diffusion coefficients converge in much shorter time spans than the mutual, this scheme can yield a prediction for D_{LiH} based on short trajectories.

We have studied the equimolar case ($x_{\mathrm{H}}=x_{\mathrm{Li}}=0.5$) in which the formula takes a very simple form. How well such a formulation will function for cases of such high density requires a careful comparison with the simulations such as given in Table III. We substitute the self-diffusion coefficients from QMD1, QMD3, and OFMD into Eq. (17) to produce composite mutual-diffusion coefficients, designated by a prefix "s." The last two columns of Table II are repeated to provide a comparison with the D_{LiH} determined from the autocorrelation function of the full mixture. At the lowest density, the results display rather erratic behavior. However, for twice solid density and above, the difference between the mutual diffusion produced from Eq. (17) and the simulations never exceeds 40% and in many cases reaches closer agreement. No particular trend emerges with density or temperature but the rule appears useful for extracting an approximate value of the mutual diffusion based on only the concentrations and the self-diffusion coefficient even in such warm dense environments.

Finally, in Table IV and Fig. 8, we show the viscosity for

TABLE III. Mutual-diffusion coefficients D_{LiH} (cm^2/s) determined from the combination of self-diffusion coefficients [D_{H}, D_{Li}] calculated from the full mixture determined by QMD1, QMD3, and OFMD simulations (prefix s). Compared to the mutual-diffusion coefficients determined from the autocorrelation function of the full mixture. Numbers in square brackets represent powers of ten.

ρ (× Solid)	T (eV)	sQMD1	sQMD3	sOFMD	QMD1	OFMD
1	2	2.1[−2]	2.0[−2]	1.9[−2]	2.2[−2]	3.4[−2]
	4	4.8[−2]	4.1[−2]	4.0[−2]	3.2[−2]	3.6[−2]
2	2	1.1[−2]	9.1[−3]	1.0[−2]	9.5[−3]	9.2[−3]
	4	2.6[−2]	2.0[−2]	2.3[−2]	2.2[−2]	3.3[−2]
	6	4.4[−2]	3.4[−2]	3.6[−2]	3.6[−2]	4.5[−2]
3	2	7.9[−3]	6.4[−3]	6.8[−3]	6.1[−3]	8.5[−3]
	4	1.9[−2]	1.5[−2]	1.5[−2]	1.6[−2]	1.9[−2]
	6	3.2[−2]	2.4[−2]	2.6[−2]	2.8[−2]	3.0[−2]
4	2	6.5[−3]	4.8[−3]	5.6[−3]	4.6[−3]	4.2[−3]
	4	1.6[−2]	1.1[−2]	1.2[−2]	1.2[−2]	1.1[−2]
	6	2.6[−2]	1.6[−2]	1.9[−2]	2.5[−2]	2.2[−2]

the QMD1 (PAW-1e) and OFMD cases as a function of density and temperature. Once again, as with the mutual diffusion, we find agreement to within 20% or better. This agreement between QMD1 and OFMD in contrast to the self-diffusion coefficients likely arises from the dominant role played by hydrogen within the mixture as evidenced by the H-H radial distribution function that shows little sensitivity to the Li PAW.

C. Mixing rules

For the static and optical properties, we found in an earlier study[9] that the MRd performed well only at the lowest

TABLE IV. Comparison of viscosities between quantum molecular dynamics with a single-electron PAW for Li (QMD) and the orbital-free molecular dynamics in the TFD mode (OFMD).

ρ (× Solid)	T (eV)	η(mPa·s) QMD1	η(mPa·s) OFMD
1	2	0.6	0.5
	4	1.3	1.0
	6		1.4
2	2	0.6	0.5
	4	1.6	1.3
	6	2.1	1.9
3	2	0.9	1.1
	4	1.3	1.2
	6	3.1	2.6
4	2	1.2	1.1
	4	2.3	1.9
	6	3.2	3.0

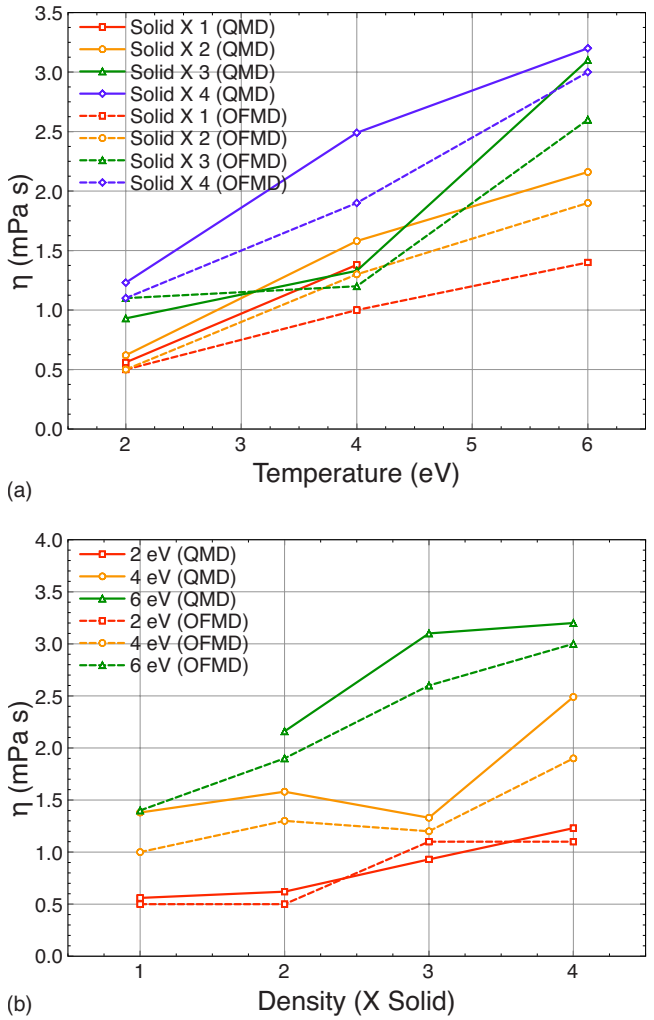

FIG. 8. (Color online) Viscosity as a function of temperature and density (top and bottom panels, respectively). Error bars are 30% or less (except for solid × 1 and 4 eV where the error is 50%)

density and temperature as expected from its ideal-gas origins. Therefore, for the dynamical processes, only the pressure rule MRp was examined. Table V presents the results

TABLE V. MRp for the mutual-diffusion coefficients for QMD as a function of density and temperature. V_H and V_{Li} are, respectively, the volumes at which $P_e[V_H,T]=P_e[V_{Li},T]$. D_H (D_{Li}) is the self-diffusion coefficient determined for a sample of 108 H (Li) atoms in a volume of V_H (V_{Li}). D_{LiH} is determined from the simple volume fraction rule. Numbers in square brackets represent powers of ten.

ρ (× Solid)	T (eV)	D_H (cm/s^2)	V_H (Å^3)	D_{Li} (cm/s^2)	V_{Li} (Å^3)	D_{LiH}^{MRp} (cm^2/s)
1	2	4.0[−2]	450	1.0[−2]	1375	1.74[−2]
	4	9.3[−2]	494	2.8[−2]	1330	4.56[−2]
2	2	2.3[−2]	262	6.2[−3]	650	1.10[−2]
3	2	1.7[−2]	185	5.7[−3]	423	9.02[−3]
4	2	1.3[−2]	146	5.2[−3]	310	7.80[−3]
	4	2.8[−2]	149	1.2[−2]	307	1.72[−2]

TABLE VI. Comparison of mixing rules for mutual-diffusion coefficients. MRp indicates the pressure mixing rule result from Table V. BIM the result from Eq. (16) with the self-diffusion coefficients from MRp. QMD1 and OFMD repeat the full-mixture results from the last two columns of Table II. Numbers in square brackets represent powers of ten.

ρ (× Solid)	T (eV)	MRp	BIM	QMD1	OFMD
1	2	1.7[−2]	1.4[−2]	2.2[−2]	3.4[−2]
1	4	4.6[−2]	4.0[−2]	3.2[−2]	3.6[−2]
2	2	1.1[−2]	9.0[−3]	9.5[−3]	9.2[−3]
3	2	9.0[−3]	8.0[−3]	6.1[−3]	8.5[−3]
4	2	7.8[−3]	7.1[−3]	4.6[−3]	4.2[−3]
4	4	1.7[−2]	1.6[−2]	1.2[−2]	1.1[−2]

for the mutual-diffusion coefficient for QMD determined by the MRp prescription outlined in Eq. (16). For each total density (V_{LiH}), we vary the H and Li volumes (V_H, V_{Li}) with 108 particles in each until the excess pressures match under the constraint that $V_{LiH}=V_H+V_{Li}$. Within these volumes, we compute self-diffusion coefficients using QMD3. Combining these according to Eq. (16) then produces the desired mutual result. The volume of H changes significantly for the mixture in order to produce the proper pressure while that of Li varies much less. This trend further supports the key role of H in these particular WDM conditions.

Finally, in Table VI, the mutual-diffusion coefficients determined for QMD1 by the MRp and the BIM prescriptions are compared with the full mixture. The BIM rule generally gives better agreement with the mixture results, remaining within 30% or better above solid density. In cases in which the MRp gives particularly large differences with QMD1, for example, at three and four times solid density at 2 eV, the BIM moves the result into better agreement.

IV. SUMMARY

We have performed a systematic study of LiH in the warm-dense-matter regime for a density range from one to four times ambient solid and for temperatures from 2 to 6.0 eV using both finite-temperature density-functional-theory QMD and OFMD. The study concentrated on dynamical properties such as diffusion and viscosity. The validity of various mixing rules, especially those utilizing pressure, were checked for composite properties determined from QMD/OFMD simulations of the pure species against calculations on the fully interacting mixture. These rules produce pressures within about 10% of the full-mixture values but mutual-diffusion coefficients as different as 50%. We found very good agreement overall between the QMD, employing a three-electron pseudopotential, and the OFMD in the Thomas-Fermi-Dirac approximation, especially at the higher temperatures and densities.

ACKNOWLEDGMENTS

We wish to acknowledge useful conversations with Brad Holian. The Los Alamos National Laboratory is operated by Los Alamos National Security, LLC for the National Nuclear Security Administration of the U.S. Department of Energy under Contract No. DE-AC52-06NA25396. Part of this work was supported by the Centre de Calcul Recherche et Technologie in Bruyres-le-Chtel.

[1] N. Santos, W. Benz, and M. Mayor, Science **310**, 251 (2005).
[2] A. Burrows, Nature (London) **433**, 261 (2005).
[3] G. Fontaine, P. Brassard, and P. Bergeron, Publ. Astron. Soc. Pac. **113**, 409 (2001).
[4] J. Paiser, J. Boyes, S. Kumpman, W. Lowdermilk, and M. Soren, Laser Focus World **30**, 75 (1994).
[5] K. Widmann, T. Ao, M. Foord, D. Price, A. Ellis, P. Springer, and A. Ng, Phys. Rev. Lett. **92**, 125002 (2004).
[6] R. Ernstorfer, M. Harb, C. Hebeisen, G. Sciaini, T. Dartigalongue, and R. Miller, Science **323**, 1033 (2009).
[7] D. Saumon and T. Guillot, Astrophys. J. **609**, 1170 (2004).
[8] J. E. Bailey, M. D. Knudson, A. L. Carlson, G. S. Dunham, M. P. Desjarlais, D. L. Hanson, and J. R. Asay, Phys. Rev. B **78**, 144107 (2008).
[9] D. A. Horner, J. D. Kress, and L. A. Collins, Phys. Rev. B **77**, 064102 (2008).
[10] S. Bastea, Phys. Rev. E **71**, 056405 (2005).
[11] J. Clérouin, V. Recoules, S. Mazevet, P. Noiret, and P. Renaudin, Phys. Rev. B **76**, 064204 (2007).
[12] J.-F. Danel, L. Kazandjian, and G. Zérah, Phys. Rev. E **79**, 066408 (2009).
[13] G. Kresse and J. Hafner, Phys. Rev. B **47**, 558 (1993).
[14] G. Kresse and J. Furthmuller, Comput. Mater. Sci. **6**, 15 (1996).
[15] G. Kresse and J. Furthmuller, Phys. Rev. B **54**, 11169 (1996).
[16] R. M. Martin, *Electronic Structure: Basic Theory and Practical Methods* (Cambridge University Press, Cambridge, 2004).
[17] F. Lambert, J. Clérouin, and S. Mazevet, Europhys. Lett. **75**, 681 (2006).
[18] S. Mazevet, F. Lambert, F. Bottin, G. Zérah, and J. Clérouin, Phys. Rev. E **75**, 056404 (2007).
[19] F. Lambert, J. Clérouin, J.-F. Danel, L. Kazandjian, and G. Zérah, Phys. Rev. E **77**, 026402 (2008).
[20] M. Brack and R. K. Bhaduri, *Semiclassical Physics* (Westview, Oxford, 2003).
[21] P. Hohenberg and W. Kohn, Phys. Rev. **136**, B864 (1964).
[22] J. P. Perdew and A. Zunger, Phys. Rev. B **23**, 5048 (1981).
[23] F. Perrot, Phys. Rev. A **20**, 586 (1979).
[24] F. Lambert, J. Clérouin, and G. Zérah, Phys. Rev. E **73**, 016403 (2006).
[25] P. Vieillefosse and J. P. Hansen, Phys. Rev. A **12**, 1106 (1975).
[26] M. P. Allen and D. J. Tildesley, *Computer Simulation of Liquids* (Oxford University Press, USA, 1989).
[27] M. Schoen and C. Hoheisel, Mol. Phys. **52**, 33 (1984).
[28] D. Alfe and M. J. Gillan, Phys. Rev. Lett. **81**, 5161 (1998).
[29] R. M. More, Adv. At. Mol. Phys. **21**, 305 (1985).
[30] P. Cade and A. Wahl, At. Data Nucl. Data Tables **13**, 339 (1974).
[31] R. Zwanzig and N. K. Ailawadi, Phys. Rev. **182**, 280 (1969).